SANDIA REPORT

SAND2010-2810
Unlimited Release
Printed May, 2010

Effect of Shell Drilling Stiffness on Response Calculations of Rectangular Plates and Tubes of Rectangular Cross-Section Under Compression

Edmundo Corona, Jhana Gorman, Jason D. Hales

Prepared by
Sandia National Laboratories
Albuquerque, New Mexico 87185 and Livermore, California 94550

Sandia National Laboratories is a multi-program laboratory operated by Sandia Corporation, a wholly owned subsidiary of Lockheed Martin Corporation, for the U.S. Department of Energy's National Nuclear Security Administration under Contract DE-AC04-94AL85000.

Issued by Sandia National Laboratories, operated for the United States Department of Energy by Sandia Corporation.

Available to DOE and DOE contractors from
U.S. Department of Energy
Office of Scientific and Technical Information
P.O. Box 62
Oak Ridge, TN 37831

Telephone: (865) 576-8401
Facsimile: (865) 576-5728
E-Mail: reports@adonis.osti.gov
Online ordering: http://www.osti.gov/bridge

Available to the public from
U.S. Department of Commerce
National Technical Information Service
5285 Port Royal Rd
Springfield, VA 22161

Telephone: (800) 553-6847
Facsimile: (703) 605-6900
E-Mail: orders@ntis.fedworld.gov
Online ordering: http://www.ntis.gov/help/ordermethods.asp?loc=7-4-0#online

SAND2010-2810
Unlimited Release
Printed May, 2010

Effect of Shell Drilling Stiffness on Response Calculations of Rectangular Plates and Tubes of Rectangular Cross-Section Under Compression

Edmundo Corona
Jhana Gorman
Jason D. Hales
Sandia National Laboratories
Albuquerque, NM 87185-0346

Abstract

This report considers the calculation of the quasi-static nonlinear response of rectangular flat plates and tubes of rectangular cross-section subjected to compressive loads using quadrilateral-shell finite element models. The principal objective is to assess the effect that the shell drilling stiffness parameter has on the calculated results. The calculated collapse load of elastic-plastic tubes of rectangular cross-section is of particular interest here. The drilling stiffness factor specifies the amount of artificial stiffness that is given to the shell element drilling degree of freedom (rotation normal to the plane of the element). The element formulation has no stiffness for this degree of freedom, and this can lead to numerical difficulties. The results indicate that in the problems considered it is necessary to add a small amount of drilling stiffness to obtain converged results when using both implicit quasi-statics or explicit dynamics methods. The report concludes with a parametric study of the imperfection sensitivity of the calculated responses of the elastic-plastic tubes with rectangular cross-section.

Acknowledgment

Thanks to Brendan Rogillio for providing us with the experimental data on the crushing of tubes of rectangular cross-section and answering our questions regarding experimental issues. Also thanks to Martin Heinstein for helpful discussions focused on the use of shell elements and to Bill Scherzinger for many helpful comments on the contents of this report. Funding was provided by the Advanced Simulation and Computing (ASC) program.

Contents

Appendix

Figures

Tables

Introduction

Shell elements allow analysts to develop relatively simple and efficient finite element models to calculate the mechanical response of thin-walled structures. The simplicity arises from the fact that the through-thickness discretization of the structure is included in the element, therefore only surface meshes need to be generated. The efficiency is a result of the reduction of the number of degrees of freedom usually required if continuum elements are used. Although the number of degrees of freedom per node is larger for the shell elements, generally the reduction in the number of nodes in a model leads to a net reduction.

The formulation of shell elements, however, is not simple. In fact, several formulations have been developed since the 1960's [1], with different levels of success. Sandia's Sierra Mechanics codes Adagio and Presto use the Key-Hoff shell element [2], which is based on the Belytschko-Lin-Tsay element [3].

The quadrilateral shell elements in Adagio and Presto have six degrees of freedom at each node (3 translational and 3 rotational). The rotations in the direction orthogonal to the plane of the shell at each node are the drilling degrees of freedom. The formulation used for these elements has no rotational stiffness in this direction. This can lead to spurious zero-energy modes of deformation similar in nature to hourglass deformation and make obtaining solutions in quasi-static problems difficult. In addition, it can lead to solution instabilities in transient explicit analysis.

These problems are addressed in Adagio and Presto by introducing artificial stiffness in the drilling degrees of freedom of the shell elements through the "drilling stiffness factor." The actual drilling stiffness used is a function of this factor, the Young's modulus of the material and the geometry of the shell element. The result can be viewed as an artificial spring that provides a reaction proportional to the amount of drilling rotation. The stiffness factor should be chosen to be small enough to add enough stiffness to allow the solver in Adagio to converge and to prevent instabilities in Presto without unduly affecting the solution. The default value for the drilling stiffness factor is zero. If difficulties are encountered with the solution, as will be demonstrated later for the problems of interest here, it is recommended to try adding a small amount of drilling stiffness. A suggested trial value for the drilling stiffness factor is 1×10^{-4} [4]. For further discussion on the drilling degree of freedom and several ways to address the issue in shell element formulations see [5] and [6].

The objective of this report is to demonstrate the effect of the shell drilling stiffness factor, and its interaction with mesh refinement, on the calculation of the post-buckling response and collapse of plate-like structures. In particular, the cases of rectangular plates under compressive edge loads and of tubes of rectangular cross-section under axial compression are considered. As a prelude, however, the case of an extensional rectangular plate under uniform transverse pressure is considered first. In all problems loading is assumed to be applied slowly so that dynamic effects are negligible. The loading period was determined accordingly when using explicit dynamics by trying various values and comparing the calculated responses until suitable loading rates were identified. At the time of this writing, the implementation of the shell drilling stiffness considered is available in the version-of-the-day (VOTD) only, but it will be included in the 4.16 release of

both Presto and Adagio.

Rectangular Plates

The effect of the shell drilling stiffness factor on the response of two rectangular plate problems is considered first. The first problem, shown in Fig. 1(a) is a linearly elastic square plate lying on the *x*-*y* plane with dimensions $a = b = 6$ in. and thickness $t = 0.120$ in. It is subjected to a uniform transverse pressure of magnitude P and is pinned at all four edges, where the in-plane deflections are also restricted. Therefore, the plate stretches as it bends. The Young's modulus and Poisson's ratio of the material are $E = 28.3 \times 10^6$ psi and $\nu = 0.3$ respectively.

The same plate geometry and material are used for the second problem, but in this case the loading is a distributed compressive edge force of total magnitude F, as shown in Fig. 1(b). The plate is still pinned at all four edges. The *x*-deflection at $x = \pm a/2$ is restricted while the *y*-deflections at $y = \pm b/2$ are prescribed to be equal and opposite. Because of the support conditions, the plate undergoes biaxial compression.

Since both problems are doubly symmetric, the models include only one quarter of the plate in the first quadrant, shown shaded in the figures. Symmetry boundary conditions are applied at $x = 0$ and $y = 0$.

Plates Under Transverse Load

When a uniform transverse pressure is applied to the plate as in Fig. 1(a), the plate will deflect into a bowl shape. Such deformation can be quantified by the transverse deflection at $(x,y) = (0,0)$, which will be called δ. Plots of pressure vs. deflection (P-δ) generated using quasi-static analysis with Adagio with different element sizes (S_E) are shown in Fig. 2(a) and (b) for values of shell drilling stiffness factor $D_s = 0$ and 1×10^{-4} respectively. All elements have unit aspect ratio. The conjugate gradient method's parameters used are shown in Table 1. Figure 2(a) shows results when elements have sizes of 1 and 0.5 in. Attempts were made to obtain results with smaller elements, but the solver failed to converge at the start of the runs. Differences between the two calculated responses can be seen, but the convergence of the results with respect to element size cannot be assessed in the absence of results with smaller elements. By contrast, when $D_s = 1 \times 10^{-4}$ the model delivered results for smaller elements as shown in Fig. 2(b). In this case the convergence of the P-δ responses can be verified since negligible difference is apparent between results obtained with 0.25 and 0.125 in. elements. Since mesh convergence was achieved, elements smaller than 0.125 in. were not considered. Clearly, setting $D_s = 1 \times 10^{-4}$ made the success of the mesh refinement study possible. A study of the effect of D_s on the performance of Adagio for this problem using 0.125 in. elements showed that a minimum value of 1×10^{-6} was needed for convergence in this case.

As expected, the P-δ responses display a hardening response due to the stretch of the plate and buildup of membrane force. For very small transverse deflections, the membrane force is small and its effect in the P-δ plot negligible. Linear analytical solutions can be easily derived (see [7]) from plate theory for the case of plates with no membrane force as summarized in Appendix A. It

is shown there that for very small deflections the nonlinear finite element calculations yield results that are virtually identical to the ones from linear plate theory.

In summary, including a shell drilling stiffness factor of 1×10^{-4} dramatically improved the convergence of Adagio's solver and allowed the mesh refinement study to complete, indicating that elements of size 0.25 in. yield converged results in this problem.

Table 1. Adagio cg solver parameters. Plates under transverse load.

Predictor scale factor	0.25
Target relative residual	1×10^{-5}
Maximum iterations	200
Adaptive stepping target iterations	50
Adaptive stepping maximum multiplier	20

Plates Under Edge Compression

Plates subjected to compressive edge loads are susceptible to buckling. If a plate is perfectly flat initially, it will remain flat under compressive edge loading until a critical value of load, the buckling load, is reached. At this point the flat configuration becomes unstable. Above this load even infinitesimally small disturbances will result in finite static displacements transverse to the plane of the plate. In reality no plate is perfectly flat, and transverse deflections develop from the beginning of loading, slowly at first, but accelerate significantly when the load approaches the vicinity of the buckling load.

The formulation of the linearly elastic plate buckling problem is presented in structural stability books such as [8]. For biaxially loaded rectangular plates the buckling load F_{cr} is given by

$$F_{cr} = k_c \frac{\pi^2}{a} \frac{Et^3}{12(1-\nu^2)} \tag{1}$$

where

$$k_c = \frac{[(na/b)^2 + m^2]^2}{(na/b)^2 + Rm^2}, \tag{2}$$

m and n are the (integer) number of buckling half-waves in the x and y directions respectively (Fig. 1(b)) and R is the ratio of the normal x-stress component to the the y-stress component ($R = \sigma_{xx}/\sigma_{yy}$). The buckling load is found by varying the values of m and n until a minimum value of k_c is determined. If the expansion of the plate in the x-direction (see Fig. 1) is prevented, then $R = \nu$, the material's Poisson's ratio, which is taken as 0.3. For a square plate, which is considered here, $a/b = 1$ and the minimum value of k_c is found when $m = n = 1$[1] and is equal to 3.077.

[1]This indicates that the buckling mode of the plate has a single half-wave in both directions, that is the mode has the shape of a bowl.

Substituting the plate dimensions and material properties given previously gives the buckling load as $F_{cr} = 22,670$ lb. The corresponding relative displacement of the edges at $y = b/2$ and $y = -b/2$, which will be called Δ, can be calculated in a straight-forward manner and is 0.00608 in.

The post-buckling response of linearly elastic rectangular plates is stable, in other words, the load continues to increase with further compressive edge displacement in spite of the growing transverse deflection. In order to study the post-buckling response of the plates numerically it is generally necessary to excite buckling by introducing a small geometric imperfection in the form of an initial lateral deflection of the unloaded plate. Without such a disturbance, the numerical solution may continue to follow the unstable equilibrium path, without lateral deflection, at loads higher than the buckling load instead of the buckled, stable path. In the results to be shown next, an initial lateral deflection in the shape of the buckling mode of the plate is introduced. The lateral deflection is in the shape of the buckling mode of the plate and is given by

$$w_o = \delta_o \cos(\pi x/a) \cos(\pi y/b) \tag{3}$$

where δ_o is the imperfection amplitude. In the results that follow $\delta_o = 0.001$ in.

Figure 3 shows the load-deflection responses calculated with Adagio for the different element sizes shown in the figure. In the cases presented, the shell drilling stiffness factor was kept fixed at 1×10^{-4} and the target relative residual at 1×10^{-9}. The solver parameters used are listed in Table 2. Figure 3(a) shows the total applied edge load F vs. the relative edge displacement Δ. The buckling load and displacement calculated from (1) and (2) are indicated by dashed lines, and their intersection defines the buckling point. The results show that for displacements under the value at buckling, the response of the plate is linear. As expected, near the buckling point the response shows a relatively fast change in slope. At higher loads the response has again a nearly constant slope. Figure 3(b) shows the total applied force vs. the lateral deflection at the center of the plate. The lateral deflection remains very small up until a load just below the buckling load, and then accelerates considerably as the load rises further. The results of the parametric study indicate that the calculated load-deflection responses become nearly identical for element sizes of 0.5 in. and below, and that the results with an element size of 0.25 in. are reasonably converged.

Setting the shell drilling stiffness factor to zero, however, can lead to severe difficulties and makes the results sensitive to the value of the target relative residual R_t, as illustrated in Figs. 4(a) and (b), which show the load as function of edge and transverse displacement calculated with 0.125 in. elements. Results obtained with $R_t = 1 \times 10^{-5}$ overshoot the buckling point and display significant roughness in the post-buckling regime. The noticeable periodic drift in the plot is often observed when convergence tolerances are too loose. A solution that is converged in one step may, in combination with the Adagio's load step predictor, be converged with few iterations in the next even though there is a noticeable drift in the solution. Changing R_t to 1×10^{-7} smooths the results considerably but not totally, and the lateral deflection of the plate now gets excited somewhat prematurely when compared to the results in Fig. 3 and to the buckling load and displacement calculations. Reducing R_t to 1×10^{-9} results in the numerical procedure not converging very early in the loading process. The last converged solution is indicated by the "$\times$" symbol in the figures.

The next step in the study was to investigate the effect of the shell drilling stiffness factor on calculations conducted using the explicit dynamics code Presto. Loading was conducted at a slow

Table 2. Adagio cg solver parameters. Plates under edge load.

Predictor scale factor	0.25
Target relative residual (R_t)	See figures
Maximum iterations	200
Full tangent preconditioner:	
Balance probe	2
Tangent diagonal scale	0.25
Adaptive time stepping:	
Target iterations	50
Maximum multiplier	20

enough rate so the results are comparable to the quasi-static predictions. As in the Adagio runs, loading was conducted by prescribing the relative displacement Δ between the edges at $y = \pm b/2$, with a maximum value of 0.02 in. The variation of Δ as a function of time is shown in Fig. 5 and is given by

$$\frac{\Delta(t)}{\Delta(T)} = \left(\frac{t}{T}\right)^3 \left[10 - 15\left(\frac{t}{T}\right) + 6\left(\frac{t}{T}\right)^2\right], \tag{4}$$

where T is the elapsed time during the run, as suggested in [9] for "smooth loading." Choosing $T = 1$ s and using a density of 0.000735 slug-ft/in^4 for the material essentially yielded the quasi-static response. The time step calculated internally by the program was used.

Graphs of the calculated load-displacement responses are shown in Fig. 6 for the cases with shell drilling stiffness factor values of 1×10^{-4} and 0, using 0.125 in. elements. The results are nearly identical up to an edge displacement of approximately 0.012 in. where the case with $D_s = 0$ deviates from the curve with $D_s = 1 \times 10^{-4}$, and subsequently predicts somewhat rough load-deflection curves that fall below the expected trends. Comparing the present results to the results obtained with Adagio in Fig. 3 shows that they fall on top of those results if $D_s = 1 \times 10^{-4}$. Therefore, it was very important to set $D_s = 1 \times 10^{-4}$ to obtain reasonable results when using Presto as well.

In summary, the results obtained for elastic rectangular plates show that it is essential to include the shell drilling stiffness factor in the analysis to be able to generate results that are reasonable, and that this holds true for both Adagio and Presto. A value of $D_s = 1 \times 10^{-4}$ gave good results in all cases. The next sections address the effect of this parameter on the more demanding calculations of the response of elastic-plastic tubes of rectangular section under axial compression.

Tubes of Rectangular Cross-Section Under Axial Compression

Several Sandia structural systems are designed to absorb kinetic energy in impact events. Beams in the structure of the safeguards transporter (SGT), for example, should be able to dissipate energy in the event of an accident. To support work related to the calculation of the response of the SGT under accident conditions, a C6 project considered the crushing and associated energy absorption of A500 steel tubes of rectangular cross-section under axial load. The experiments were conducted under quasi-static loading conditions, and the results were documented in [10].

Figure 7 shows two of the tested specimens. The specimen in Fig. 7(a) had nominal outer cross-sectional dimensions 6×3 in., nominal thickness of 0.120 in. and length of 48 in. The tubes had a longitudinal weld seam and were held at both ends using custom-made fixtures consisting of a rectangular cavity with a depth of 2 in. where the specimens fit snugly. No internal support was provided to the tubes at these fixtures. Loading was achieved by holding one end of the specimens fixed while prescribing the displacement of the other in the direction of the specimen axis at a rate of 1 in/min. This tube collapsed by localized crushing at the lower end. The photograph shows two well-defined folds. Figure 8(a) plots the axial load-deflection (F-Δ) response of the specimen in Fig. 7(a). It is characterized by significant load fluctuations as each fold formed and came into contact with the preceding fold, or perhaps the gripping fixture in the case of the first fold. The part of interest in this study, however, encompasses only the first load peak, which represents the maximum load that the tube can take and therefore is the collapse load of the tube. A close-up of the measured response in this regime is shown in Fig. 8(b). Although one would expect an initially linear F-Δ response, flexibility and backlash in the experimental apparatus is the most likely source of the initial nonlinearity. Eventually a limit load developed in the response as the tube started collapsing. Further compression occurred under decreasing load as the first fold developed. All specimens of similar geometry and length had very similar responses. Specimens of shorter length, 20 in., displayed the same type of collapse mode. A total of ten 48 in. specimens and eight 20 in. specimens were tested.

Figure 7(b) shows a specimen that collapsed in a global mode and developed a kink near the mid-span of the beam. The gripping and loading conditions were similar as in the case discussed previously. This specimen had nominal cross-sectional dimensions 2×2 in., thickness of 0.083 in and length of 44 in. The measured F-Δ response is shown in Fig. 9(a) and shows a load maximum followed by a significant load decrease up until a displacement of approximately 3 in. followed by a very small load increase probably due to self-contact in the kink region. Again, the regime of interest is the beginning of the response, up until a little after the load maximum, as shown in Fig. 9(b). For the current cross-sectional geometry, most of the specimens of length 44 in. collapsed in the mode shown in Fig. 7(b), but shorter specimens of length 20 in. tended to collapse by progressive crushing. A total of seven 44 in. specimens and seven 20 in. specimens were tested.

Material characterization of A500 steel through uniaxial tension tests was carried out in [11]. The test coupons did not come from tube material, but rather from structural hat sections of the same material. Tests were conducted for longitudinal and transverse cuts at different temperatures and strain rates. The stress-strain curve used in the calculations that follow is shown in Fig. 10 up to a strain of 5%. A multilinear fit was conducted. The circles in the figure represent the enpoints

of the linear segments. This tension test was conducted quasi-statically at an approximate strain rate of 0.16% per second. The measured Young's modulus, E, and the 0.2% strain offset yield stress, σ_o, are given in the figure.

The next section of this report will address the predictions of initial collapse including the effect of element size and of the value of the shell drilling stiffness factor for the $6 \times 3 \times 0.120$ in. columns. The effect of the value of the shell drilling stiffness factor on the response assuming linearly elastic material is shown first as a small prelude to the consideration of the elastic-plastic response. A parametric study of the imperfection sensitivity of the elastic-plastic response of both column geometries concludes the report.

Local Buckling

Local buckling or collapse refers to instances where large deformations occur over a relatively small region of a structural member while the rest of the member has significantly smaller deformations. In elastic-plastic buckling problems, these large local deformations start growing at approximately the same time as the load borne reaches a maximum value and develop as the load decreases. Since all $6 \times 3 \times 0.120$ in. columns tested collapsed locally, this geometry will be used to study the performance of both Adagio and Presto when modeling local collapse.

As was done in the section on buckling of plates, a small geometric imperfection will be introduced in the model of the tubes to seed the post-buckling deformations and later study their imperfection sensitivity. The geometric imperfection has two components: one in the plane of the cross-section and one along the axis of the tube. The shape of the imperfection in the cross-section is shown in Fig. 11. It is characterized by a bowing of each side of the tube in the shape of a half sine wave. The amplitude of the imperfection is given by w_o on two of the sides. To keep the sides at 90° to each other at the corners, the imperfection amplitude at the other sides is αw_o where $\alpha = a/b$, the ratio of the length of the sides. The variation of the imperfection along the tubes is also sinusoidal with half-wavelength λ, which is prescribed. In the cases considered here, the value of λ is a small fraction of the length of the tube.

Obviously, the imperfection shape being considered is very simple compared to what could be expected in reality. In a testing environment, imperfections can arise due to deviations from flatness of the tube's wall arising from tolerances in the manufacturing process or from impact during handling and transportation. Additionally, the axis of the tube may not be perfectly straight, the testing machine can have slight misalignments and some differences in boundary conditions between test and those idealized in the analysis exist. None of these factors are known. Therefore, the initial geometric imperfection considered in the analysis is useful only to investigate the sensitivity of the collapse loads of the tubes to the magnitude of imperfections, but it is not meant to represent an imperfection that was actually present in the tests. The effect of the two imperfection parameters, amplitude and wavelength, will be addressed later in this report.

Figure 12 shows an example of the mesh used to model the tubes. It includes only one-half of the tube. A single plane of symmetry with normal along the y direction that cuts the 6 in. sides in

Table 3. Adagio cg solver parameters. Tube collapse cases.

Predictor scale factor	1.0
Maximum iterations	1000
Minimum iterations	0
Line search	Tangent
Full tangent preconditioner:	
Balance probe	2
Linear solver	feti
Tangent diagonal scale	0.01
Adaptive time stepping:	
Target iterations	100
Maximum multiplier	20
Minimum multiplier	0.001

half is used. Although the imperfection and expected deformation will also be symmetric about a plane through the center of the tube and with normal along the x direction, that was neglected because a latter section will address the possibility of column buckling type deflections that are not symmetric about this plane. The periodic nature of the initial imperfection can be appreciated in this figure.

When using Adagio, the solver parameters used that are common to all cases run are given in Table 3. The parameters varied in this study include the relative target residual, the value of the shell drilling stiffness factor and the size of the shell elements. In all cases the elements have nominally unit aspect ratio and uniform size throughout the model. Small deviations from these rules occur because the dimensions of the mid-surface of the tube are not round numbers.

The reminder of this section will address the response of the tubes starting with a brief discussion of the linearly elastic case and followed by consideration of the elastic-plastic response. In all cases presented, the length of the tubes was kept at 24 in. Although tubes of this length were not tested, using this length was convenient for the study of the effect of element size in the response. The amplitude and half-wavelength of the imperfection were constant with values $w_o = 0.0125$ in. and $\lambda = 1$ in. respectively. Results obtained with Adagio will be presented first, followed by results obtained with Presto. In all cases, both ends of the tube were pinned, that is the deflection components perpendicular to the tube axis were zero, but the rotations were left free. Loading was accomplished by restricting the axial deflection at one end of the tube and prescribing it at the other end. The axial force F was calculated by summing the nodal reactions at one end and then doubling the sum on account of symmetry.

Results with Implicit Quasi-Statics. Adagio

Figure 13 shows the calculated axial load-deflection (F-Δ) response of the tubes when the shell drilling stiffness factor has values of $D_s = 0$ and 1×10^{-4}, and the material was linearly elastic.

The element size was $S_E = 0.125$ in. and the target relative residual $R_t = 1 \times 10^{-7}$. The effect of element size will be addressed later, in conjunction with the elastic-plastic case. The results show that the case with $D_s = 0$ failed to converge very early in the process, at the place indicated by "$\times$" in the figure. Setting $D_s = 1 \times 10^{-4}$ yielded results that ran to completion. The shape of the load-deflection response is qualitatively very similar to that of flat plates. The deformed mesh at an axial displacement $\Delta = 0.12$ in. is shown in Fig. 14 and shows a periodic deformation with 5 half-wavelengths along the tube.

Figure 15 shows, for different element sizes, the calculated load-deflection response if the material is elastic-plastic with the uniaxial stress-strain curve in Fig. 10. The plasticity model is based on flow theory, is rate independent and hardens isotropically. The shell drilling stiffness factor was kept at $D_s = 1 \times 10^{-4}$; setting it to zero caused the nonlinear solver to diverge prior to achieving the limit load, except when the largest element considered, 1 in., was used.

Clearly, including the elastic-plastic behavior of the material changes the axial load-deflection response significantly. Now the response is characterized by a load maximum, so the structure will collapse if loads higher than the maximum are attempted. Therefore, the load maximum represents the collapse load of the tube. In the calculations, the axial displacement at one end of the tube was prescribed, so the post-collapse response could be calculated.

The figure shows that the load-deflection responses converged rapidly as the element size decreased, and that for elements smaller than 0.25 in. the results are almost indistinguishable. Figure 16 shows a plot of the calculated dependence of the collapse load as a function of the number of elements along the 24 in. length of the tube and compares them to similar calculations obtained using the commercial program Abaqus/Standard using an equivalent shell element (S4R) [9]. The results from both codes are convergent, very similar, and the difference reduces as the element size decreases. Using elements of size 0.25 in. (96 elements along the length) or smaller yields reasonable results.

The effect of varying the value of D_s in steps of two orders of magnitude on the calculated axial load-deflection response is shown in Fig. 17. The results show that a minimum value of 1×10^{-10} is needed to calculate the maximum load in the response. Interestingly, the maximum load increases as the value of D_s increases. Each of the calculated curves look reasonable by itself, with the exception of the case with $D_s = 1$, which predicts a post-limit-load response that includes a rising load not seen in practice. Based on the information presented, it is difficult to determine what a converged value of D_s is. Perhaps a hint of a reasonable value is pointed out by the fact that the minimum difference in the calculated maximum load occurred between $D_s = 1 \times 10^{-4}$ and 1×10^{-2}. The difference between these two cases was 0.1%. These two curves are almost indistinguishable in Fig. 17 and suggest setting the value of D_s in this range.

As one may perhaps expect, the S4R element in Abaqus also includes an artificial stiffness associated with the shell drilling degree of freedom. Although the Abaqus Theory Manual [12] is not explicit with respect to the drilling stiffness implementation for the S4R element, in other shell elements their algorithm constrains the rotation about the shell normal to match the in-plane rotation measured from the displacement field. This may be similar to the method presented in [5]. According to the user's manual [9] the default value of this stiffness has been calibrated to deliver

good results in most cases, but the user is allowed to modify it via a scaling factor. The default value was used in all Abaqus calculations. The agreement on the calculated maximum loads between Abaqus/Standard and Adagio was best when $D_s = 1 \times 10^{-4}$. In view of the observations mentioned in this and the previous paragraph and the recommendation in [4], a value of $D_s = 1 \times 10^{-4}$ is adopted for the rest of the report unless otherwise stated.

Results with Explicit Dynamics. Presto

The collapse calculations were repeated using explicit dynamics. As in the case of the plate, the axial displacement is prescribed according to the function shown in Fig. 5 with $\Delta(T) = 0.12$ in. and $T = 0.1$ s. The results for the elastic cases corresponding to those shown in Fig. 13 are shown in Fig. 18. When the shell drilling stiffness factor is $D_s = 1 \times 10^{-4}$, the results are essentially identical to those obtained with Adagio. When $D_s = 0$, however, the explicit calculations yield results that run to completion, but similarly to the plates, the calculated load is significantly lower once $\Delta > 0.04$ in.

The effect of element size on the elastic-plastic calculations with $D_s = 1 \times 10^{-4}$ are shown in Fig. 19. The trend is very similar to the one obtained with Adagio although the shapes of the axial load-deflection curves are somewhat different after passing the load maxima. In fact, the calculated limit loads by Adagio and Presto are compared in Fig. 20 as functions of the number of elements along the tube and are almost identical. The difference in the shape of the post-buckling load-deflection responses can be eliminated by increasing T to 1 s as shown in Fig. 21. Note that for all three values of T, the curves are identical up to the maximum load.

Whereas setting $D_s = 0$ in Adagio caused the numerical procedure to diverge for element sizes 0.5 in. or smaller, calculations using Presto can run to completion when $D_s = 0$, as was the case when the material was linearly elastic. The results obtained here also display erratic behavior that accentuates as the element size decreases. Figure 22 shows a comparison of the collapse loads calculated with $D_s = 0$ and 1×10^{-4}. Clearly, the results obtained with $D_s = 0$ are non-convergent since the calculated collapse loads continue to decrease significantly as the element size decreases (or the number of elements along the length increases).

The values of the predicted maximum loads calculated with Presto follow a similar trend as the results obtained with Adagio when varying the value of D_s. Interestingly, the maximum loads calculated with Presto when $D_s = 0$ and with Adagio when $D_s = 1 \times 10^{-10}$ (the smallest D_s that allowed calculation of the load maximum) are virtually identical. This suggests that results calculated with Adagio with values of D_s just large enough to allow calculation of the limit load may also show a lack of mesh size convergence similar to that displayed by Presto when $D_s = 0$.

Imperfection Sensitivity and Lateral Buckling

It is well known that the response of thin-walled structures can be imperfection sensitive. Studying the imperfection sensitivity is especially important when a load maximum is present,

as was the case for the elastic-plastic tubes considered so far. The geometric imperfection that has been considered to this point consists of a periodic wrinkle along the tube. It has two parameters: the wavelength (λ) and the amplitude (δ_o). Only numerical results for $6 \times 3 \times 0.120$ in. tubes using $\lambda = 1$ in. and $\delta_o = 0.0125$ in have been presented so far. In the following, we consider first a brief study of the sensitivity of the collapse load of such tubes to these two parameters and then conclude with consideration of a global, column-type lateral buckling mode such as that observed in $2 \times 2 \times 0.083$ in. columns (see Fig. 7(b)). All calculations in this section are conducted quasi-statically with Adagio.

The effect of changing the wavelength of the imperfection for $6 \times 3 \times 0.12$ in. columns on their collapse load is shown in Fig. 23 using element sizes $S_E = 0.25$ and 0.125 in. when $\lambda = 0.5$, 1 and 2 in. The results show sensitivity to λ with a minimum collapse load predicted for the case with $\lambda = 1$ in. for both element sizes. This value was used for all other calculations for tubes with similar cross-sectional dimensions since it was conservative. The effect of varying δ_o on the axial load-deflection response is shown in Fig. 24. The results indicate that the collapse load of the columns is indeed imperfection sensitive since an imperfection of amplitude $\delta_o = 1/16$ in. can reduce the collapse load by approximately 40%. Using $\delta_o = 0.0125$ in. approximately matches the collapse loads measured experimentally, which ranged between 85 and 100 kips. Another point of interest is that even the column with no imperfection displayed collapse, indicating that there is sufficient numerical "noise" in the solution to trigger buckling and collapse. This is not always guaranteed.

Although progressive crushing, which starts as local collapse, was the only mode observed in the $6 \times 3 \times 0.12$ in. columns tested, it is natural to consider the possibility of a global column-type buckling mode that leads to global collapse, as in Fig. 7(b) for $2 \times 2 \times 0.083$ in. columns. The rest of this section will concentrate on the interaction between these two possible modes of collapse. As with local collapse, the global mode can be excited by a suitable geometric imperfection. Since the supports at the ends of the columns in the experiments approach a clamped boundary condition for global deflections, the initial imperfection used consists of a lateral deflection in the global x-direction without cross-sectional distortion given by

$$u_x = \frac{\delta_c}{2}\left[1 - \cos\left(\frac{2\pi z}{L}\right)\right]. \tag{5}$$

The two imperfections are then added to produce the initial geometry of the mesh.

Whereas progressive crushing dominated the behavior of all $6 \times 3 \times 0.12$ in. tubes in the experiments, the behavior of the $2 \times 2 \times 0.083$ in. tubes was strongly dependent on the specimen length. Most tubes with $L = 20$ in. crushed progressively whereas most of the longer tubes with $L = 44$ in. displayed large global displacements, as in Fig. 7(b). Hence, these cases present a good opportunity to study the interaction between the two collapse modes and therefore between the effect of the two imperfection shapes.

Figure 25 shows the axial load-deflection response of columns with $L = 20$ in. In this figure, the periodic imperfection parameters were kept constant at $\lambda = 0.5$ in. (determined through parametric studies similar to those shown in Fig. 23) and $\delta_o = 0.0083$ in. while the amplitude of the global imperfection was varied between 0 and 1 in. The results show that when the column imperfection is

very small ($\delta_c < 0.1$ in.), the presence of the lateral imperfection has a negligible effect on the load-deflection curves and the deformation localizes at one end of the column in a manner similar to that shown in Fig. 26(a). For larger values of δ_c the shapes of the response curves begin to change, as the column-type imperfection influences the response more significantly and the deformations show increasing lateral deflections as shown in Fig. 26(b) when $\delta_c = 0.25$ in. Note that although the lateral deflection is significant, regions where localized deformation at the ends and center of the column are present. Whether progressive crushing or global deflections will eventually dominate the response at very large axial displacement requires extending the calculations to that regime, but that is beyond the scope of the present report.

Results when the columns have $L = 44$ in. are shown in Fig. 27. Here the character of all the curves, except the one with $\delta_c = 0$ are similar and are mostly influenced by the lateral deflection of the columns, as seen by inspecting the deflected shapes at the conclusion of the runs. The exception is the curve corresponding to $\delta_c = 0$, which displays a sudden load drop. Interestingly, no lateral deformations developed in this case. Instead, a local buckle developed at one end. The results indicate that the global collapse mode is strongly preferred by the $2 \times 2 \times 0.083$ in. columns with $L = 44$ in., but also that it is important to include an appropriate initial geometric imperfection to obtain the correct response.

The collapse load measured in the experiments for $2 \times 2 \times 0.083$ in. columns were in the range of 25 to 30 kips for both lengths. The lateral imperfections required to yield calculated collapse loads in this range are in the vicinity of 0.25 in. Results not presented in this report indicate that the amplitude of a periodic wrinkle type imperfection on its own would have to be in the range of 0.05 in. to bring the calculated maximum loads to the range seen in the experiments. These values seem large. Recall, however, that the yield stress of the material is uncertain since it was not measured on coupons extracted from the same material batch as the tubes tested. Hence it is difficult to assess a reasonable value of amplitude for the imperfections.

Summary and Conclusions

This report concentrated on the effect of shell drilling stiffness on the calculation of the pre- and post-buckling responses of flat rectangular plates and tubes of rectangular cross-section under slowly applied compression. These problems were very sensitive to the inclusion of the artificial stiffness associated with the drilling degree of freedom in the shell elements used. Keeping the drilling stiffness factor at zero (which is the current default value in Adagio and Presto) made convergence of the conjugate gradient method in Adagio difficult to achieve, especially if the element sizes were relatively small. On occasion, the method produced solutions, but the results obtained were strongly dependent on the solver parameters and, in general, unreliable. Calculations conducted with the explicit dynamics program Presto generally produced results, but the lack of drilling stiffness resulted in numerical errors that were not always obvious but led to erroneous results. In the case of elastic-plastic tubes of rectangular cross-section the erroneous results only became apparent when conducting a mesh convergence study. In that case, refining the mesh did not lead to convergence of the calculated collapse load of the tubes.

Including the recommended value for the shell drilling stiffness factor ($D_s = 1 \times 10^{-4}$) greatly improved the performance of the element and eliminated all the numerical errors previously mentioned. The comparison of results between the two Sierra programs and the commercial code Abaqus/Standard (with its default value for the drilling stiffness) was excellent. Whether the problems considered in this report were particularly sensitive to the value of the shell drilling stiffness factor, perhaps because of their piecewise nearly flat geometries, or if any shell model will display this sensitivity has not been addressed here. At this point the sensitivity of shell model predictions to the value of drilling stiffness factor should be tested in a case-by-case basis.

Finally, Adagio was used to conduct a parametric study of the imperfection sensitivity of the collapse behavior of elastic-plastic tubes of different cross-sections. The calculated collapse loads (load maxima in the response) fell in the range of the experimentally measured ones when reasonable values of initial imperfections were used for the $6 \times 3 \times 0.120$ in. columns. The imperfection amplitudes required to predict collapse loads that were close to experimental values for the $2 \times 2 \times 0.083$ in. columns seemed larger than expected. The collapse loads, however, are also dependent on the material properties, which are uncertain since they were not measured from coupons extracted from actual test specimen material. By combining two types of initial geometric imperfections, one that would favor local collapse and another that would favor global collapse, it was possible to estimate the dependence of the collapse modes of $2 \times 2 \times 0.083$ in. tubes on their lengths as observed experimentally.

A Analytical Solution for Plates under Transverse Pressure

The linear differential equation for bending of rectangular elastic plates with no in-plane loads is relatively easily derived in textbooks such as [7]. If w is the transverse deflection of a plate of thickness t that lies in the x-y plane and is subjected to a pressure P as in Fig. 1(a), the governing equation is

$$\frac{\partial^4 w}{\partial x^4} + \frac{\partial^4 w}{\partial x^2 \partial y^2} + \frac{\partial^4 w}{\partial y^4} = P/D \tag{6}$$

where

$$D = \frac{Et^3}{12(1-\nu^2)}. \tag{7}$$

E and ν are the Young's modulus and Poisson's ratio of the material, respectively.

If the plate is pinned at all four edges, the boundary conditions are

$$w(\pm a/2, y) = w(x, \pm b/2) = \frac{\partial^2 w(\pm a/2, y)}{\partial x^2} = \frac{\partial^2 w(x, \pm b/2)}{\partial y^2} = 0, \tag{8}$$

and the solution can be expressed in terms of a double trigonometric series that converges rapidly. The maximum deflection for a square plate ($a = b$), which occurs at the center, is calculated as

$$\delta = \frac{0.0443 P a^4}{Et^3} \tag{9}$$

by taking the first four non-zero terms in the series.

Figure 28 shows a comparison of the deflection calculated with Adagio and with (9). As expected, the analytical and the finite element solutions agree when the deflections are very small.

References

[1] MacNeal, R.H., "Perspective on Finite Elements for Shell Analysis," *Finite Element Analysis and Design*, **30**, pp. 175–186, 1998.

[2] Key, S.W. and Hoff, C.C., "An Improved Constant Membrane and Bending Stress Shell Element For Explicit Transient Dynamics," *Computer Methods in Applied Mechanics and Engineering*, **124**, pp. 33–47, 1995.

[3] Belytschko, T., Lin, J.I. and Tsay, C.S., "Explicit Algorithms for the Nonlinear Dynamics of Shells," *Computer Methods in Applied Mechanics and Engineering*, **42**, pp. 225-251, 1984.

[4] Presto VOTD User's Guide. Draft, January 18, 2010.

[5] Kanok-Nukulchai, W., "A Simple and Efficient Finite Element for General Shell Analysis," *International Journal for Numerical Methods in Engineering*, **14**, pp. 179–200, 1979.

[6] Zhu, Y. and Zacharia, T., "A New One-Point Quadrature, Quadrilateral Shell Element with Drilling Degrees of Freedom," *Computer Methods in Applied Mechanics and Engineering*, **136**, pp. 165–203, 1996.

[7] Oden, J.T. and Ripperger, E.A., Mechanics of Elastic Structures, 2nd Edition, McGraw-Hill, 1981.

[8] Brush, D.O. and Almroth, B.O., Buckling of Bars, Plates and Shells, McGraw-Hill, 1975.

[9] Abaqus Analysis User's Manual. Version 6.9, 2009.

[10] Rogillio, B., "SGT Beam Buckling," Test Memo, Sandia National Laboratories, 2005.

[11] Rogillio, B., "SGT Material Characterization," Test Memo, Sandia National Laboratories, 2004.

[12] Abaqus Theory Manual. Version 6.9, 2009

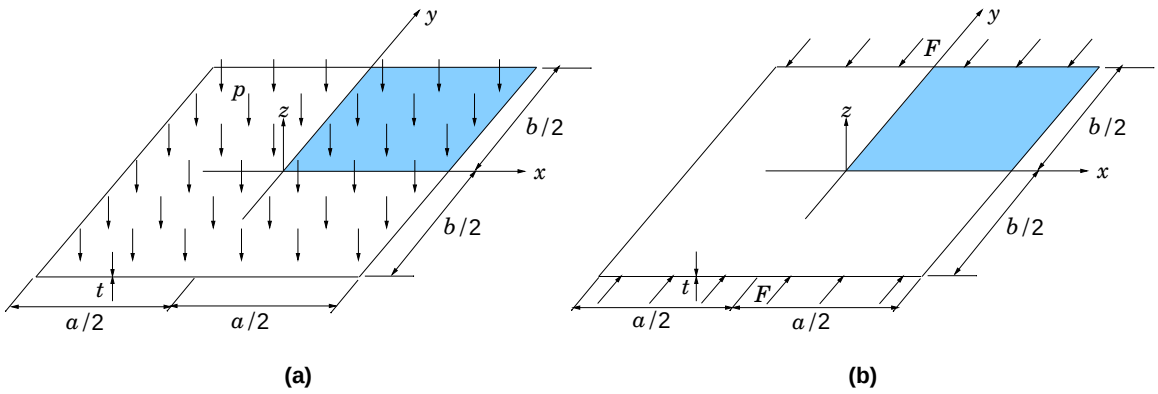

Figure 1. Plate geometry and applied loads for the problems considered. Edge loads that develop due to the support conditions are not shown. (a) Transverse loading and (b) edge compressive load.

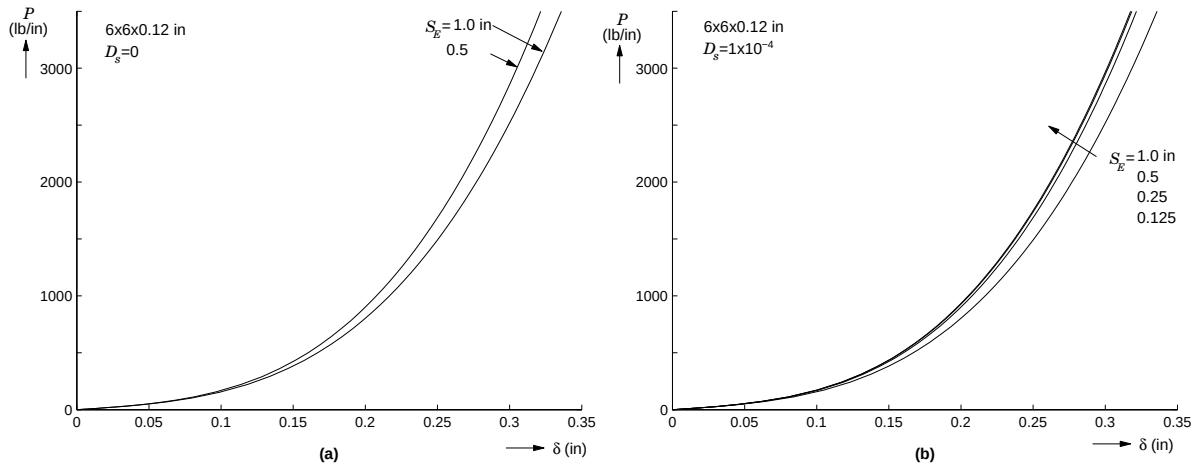

Figure 2. Transverse pressure vs. transverse displacement response of a $6 \times 6 \times 0.12$ in. plate calculated with implicit quasi-statics (Adagio) for several element sizes. (a) Zero shell drilling stiffness factor (cases with $S_E \leq 0.25$ in. failed to converge) and (b) shell drilling stiffness factor set to 1×10^{-4}.

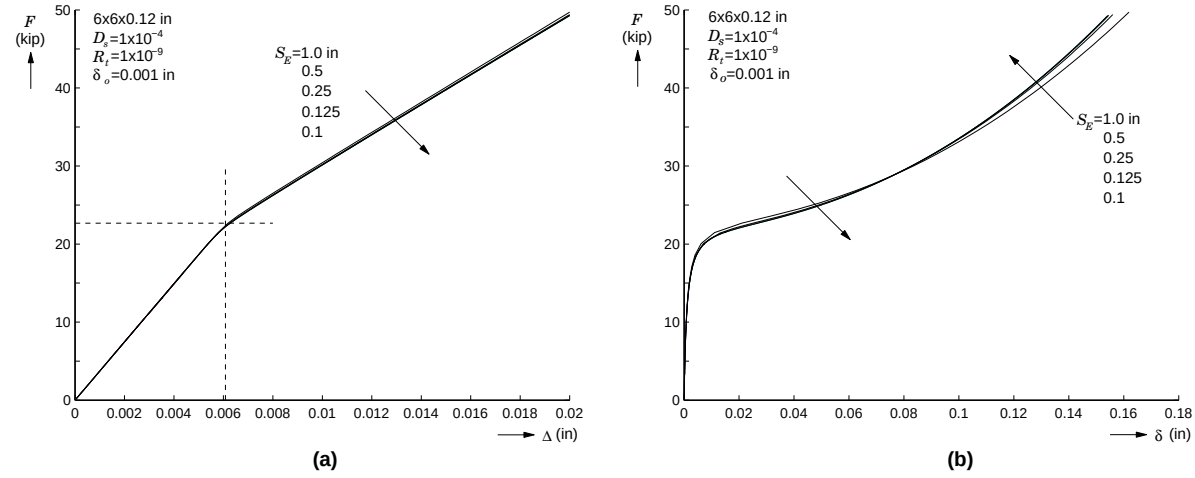

Figure 3. Calculated quasi-static response of a $6 \times 6 \times 0.12$ in. plate subjected to compressive edge loading with shell drilling stiffness factor of 1×10^{-4} and different element sizes. (a) Force vs. in-plane edge displacement and (b) Force vs. transverse displacement at the center of the plate.

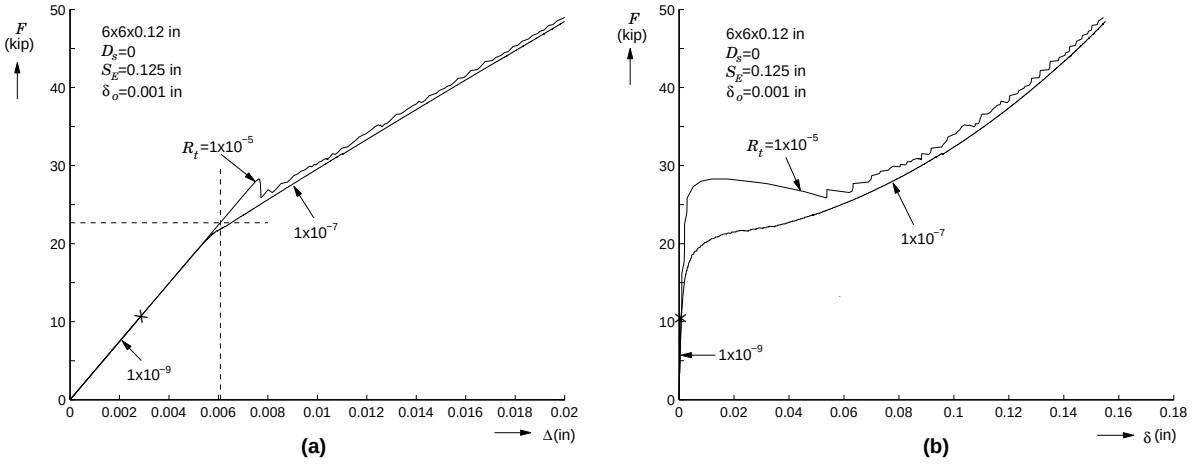

Figure 4. Calculated quasi-static responses of a $6 \times 6 \times 0.12$ in. plate subjected to compressive edge loading with no shell drilling stiffness and 0.125 in. element size for different values of target relative residual tolerance. (a) Force vs. in-plane edge displacement and (b) Force vs. transverse displacement at the center of the plate.

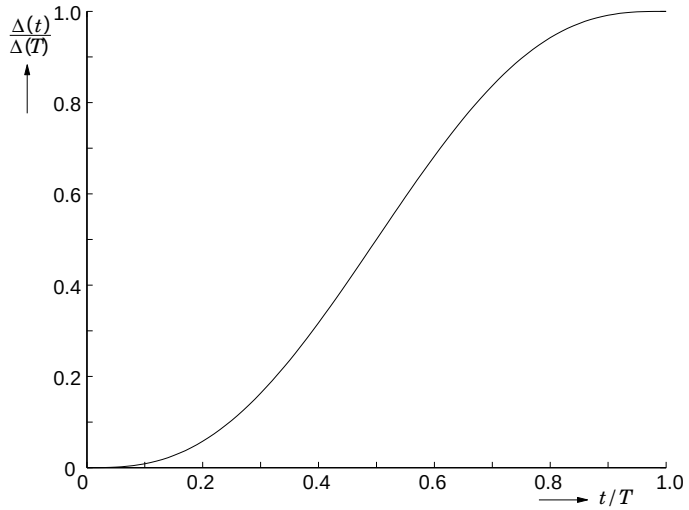

Figure 5. Loading function for Presto.

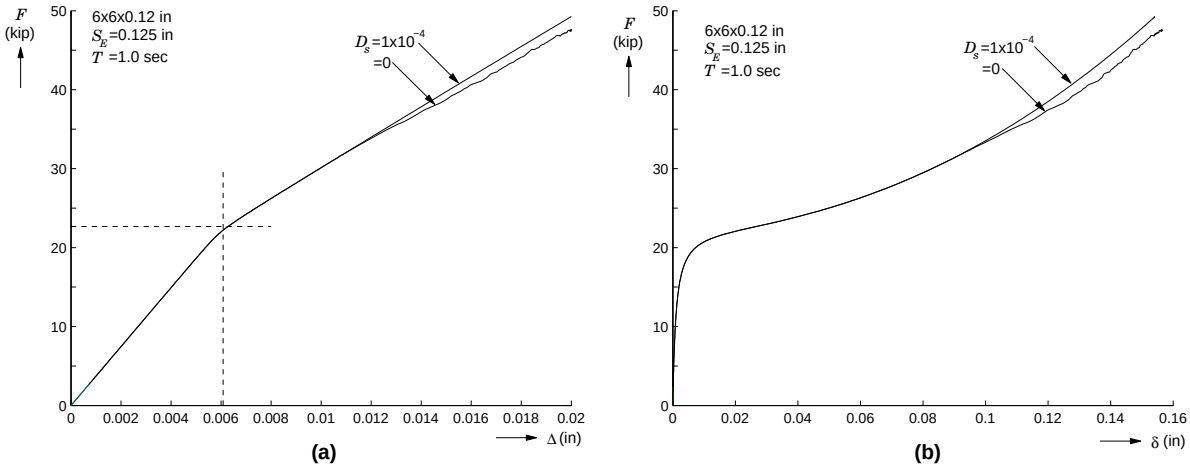

Figure 6. Response of a $6 \times 6 \times 0.12$ in. plate subjected to compressive edge loading calculated with explicit dynamics (Presto) with shell drilling stiffness factor of 1×10^{-4} and zero. (a) Force vs. in-plane edge displacement and (b) Force vs. transverse displacement at the center of the plate.

(a) (b)

Figure 7. Collapse modes. (a) Progressive crushing in a $6 \times 3 \times 0.12$ in. specimen with length of 48 in. and (b) global symmetric in a $2 \times 2 \times 0.083$ in. specimen with length of 44 in.

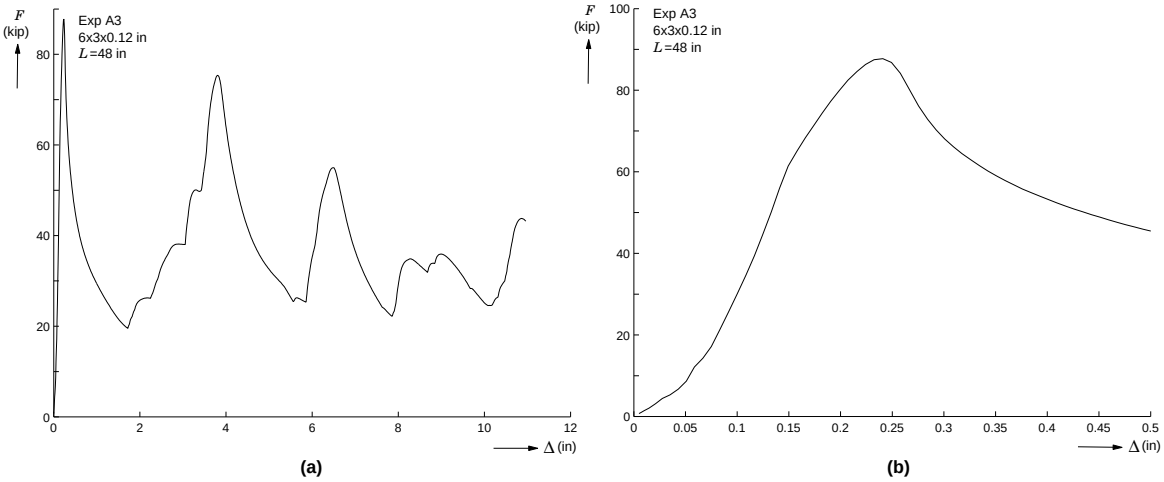

Figure 8. Axial load-deflection response the $6 \times 3 \times 0.120$ in. specimen in Fig. 7(a). (a) Complete response and (b) close-up of the initial part.

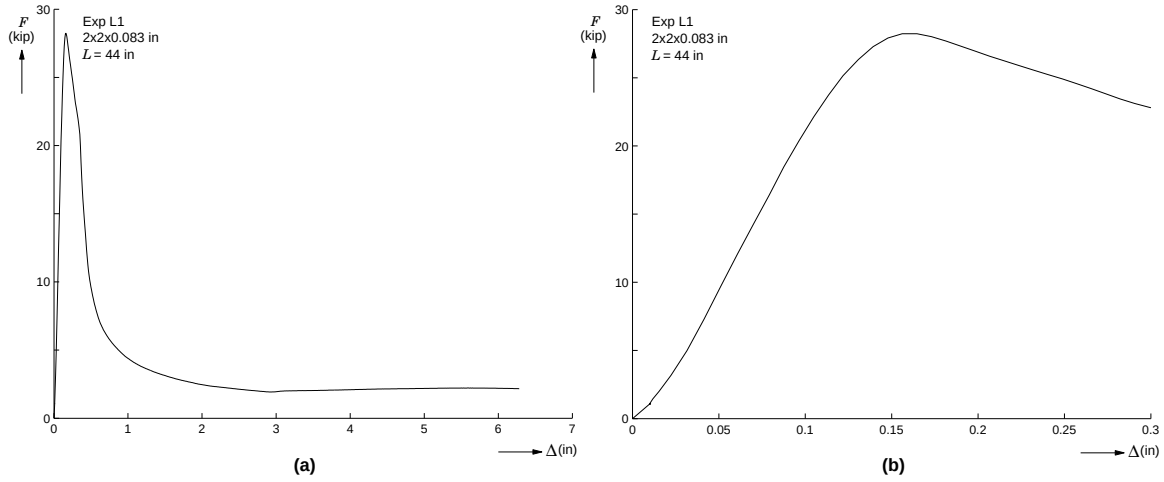

Figure 9. Axial load-deflection response the $2 \times 2 \times 0.083$ in. specimen in Fig. 7(b). (a) Complete response and (b) close-up of the initial part.

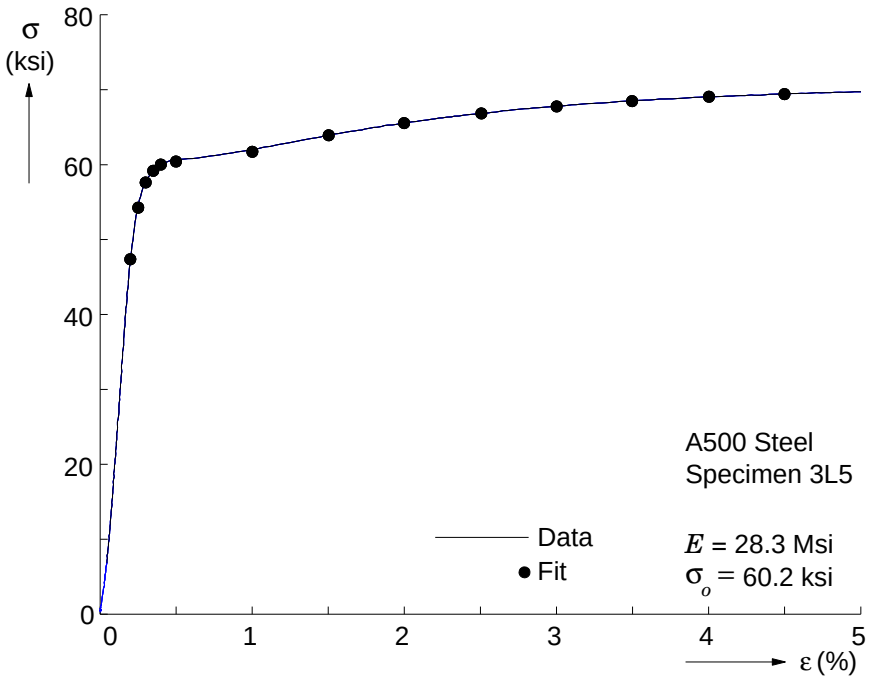

Figure 10. Uniaxial stress-strain curve for A500 steel and points picked for multilinear fit.

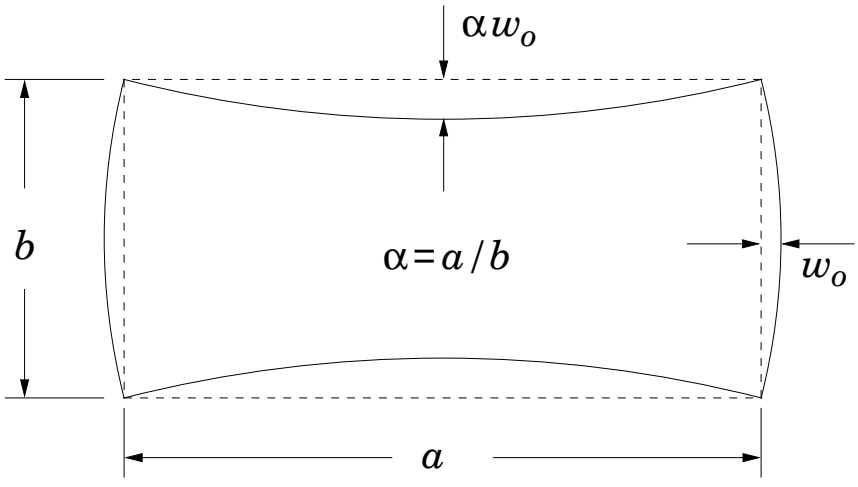

Figure 11. Imperfection shape in the plane of the cross-section.

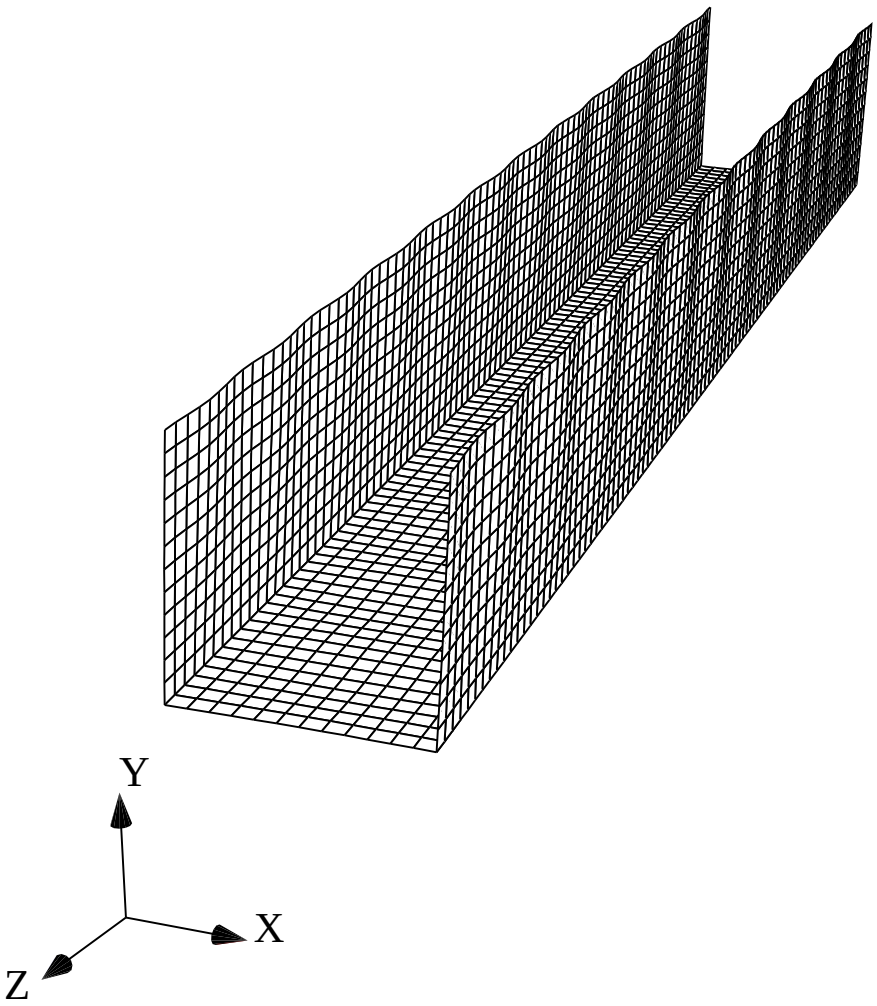

Figure 12. Model mesh for $6 \times 3 \times 0.120$ in tubes. The model represents one-half of the tube on account of symmetry. Elements of size 0.25 in. are shown.

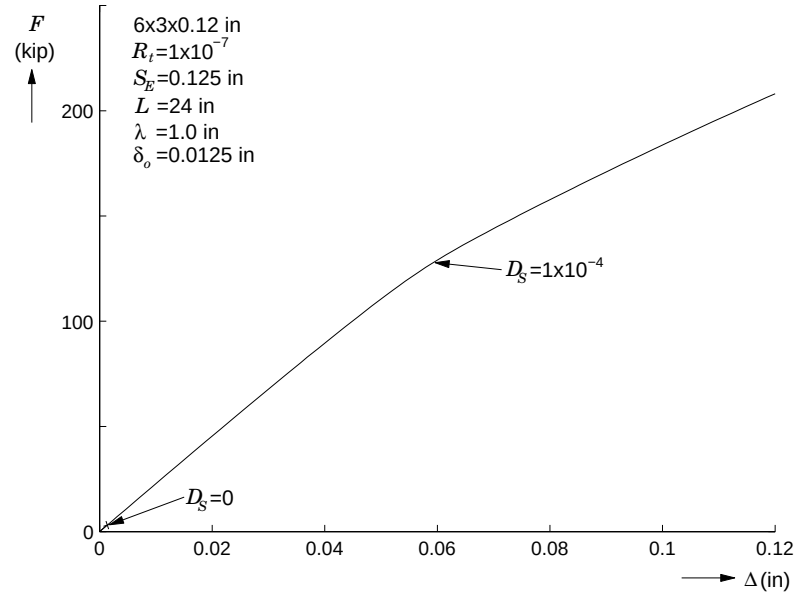

Figure 13. Calculated axial load-deflection response for a 24 in. long, linearly elastic $6 \times 3 \times 0.12$ in. tube using two values of shell drilling stiffness factor.

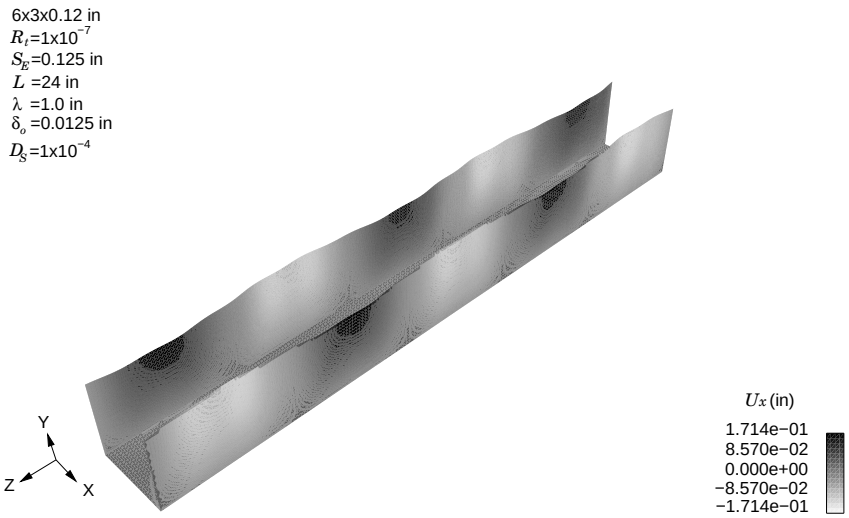

Figure 14. Shape of a 24 in. long, $6 \times 3 \times 0.12$ in. linearly elastic tube when the axial displacement is $\Delta = 0.12$ in.

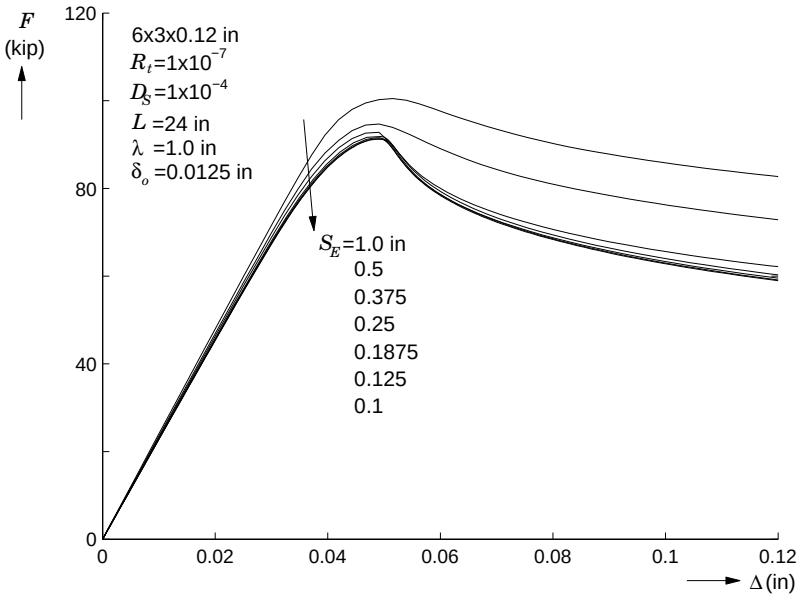

Figure 15. Comparison of the quasi-static axial load-deflection responses calculated for a 24 in. long, elastic-plastic $6 \times 3 \times 0.12$ in. tube with different element sizes.

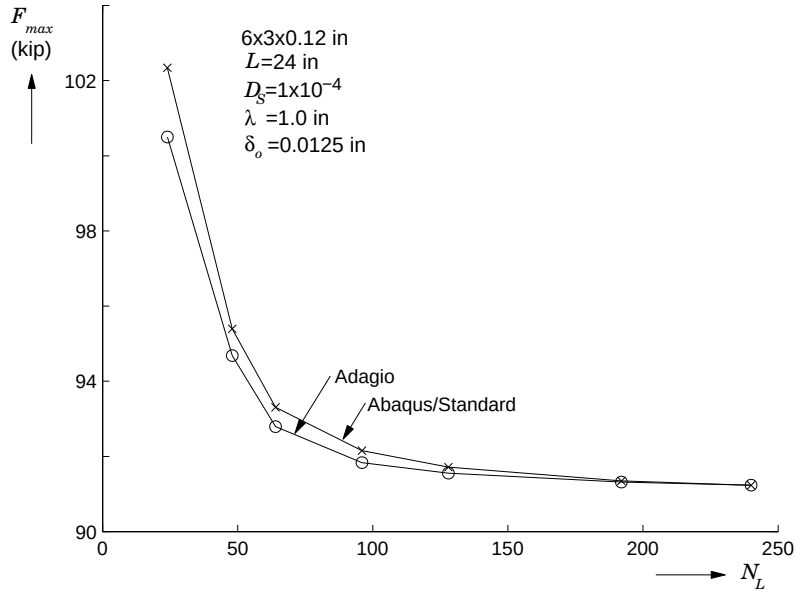

Figure 16. Comparison of the limit loads predicted for 24 in. long, $6 \times 3 \times 0.12$ in. tubes by Adagio and Abaqus/Standard for different element sizes.

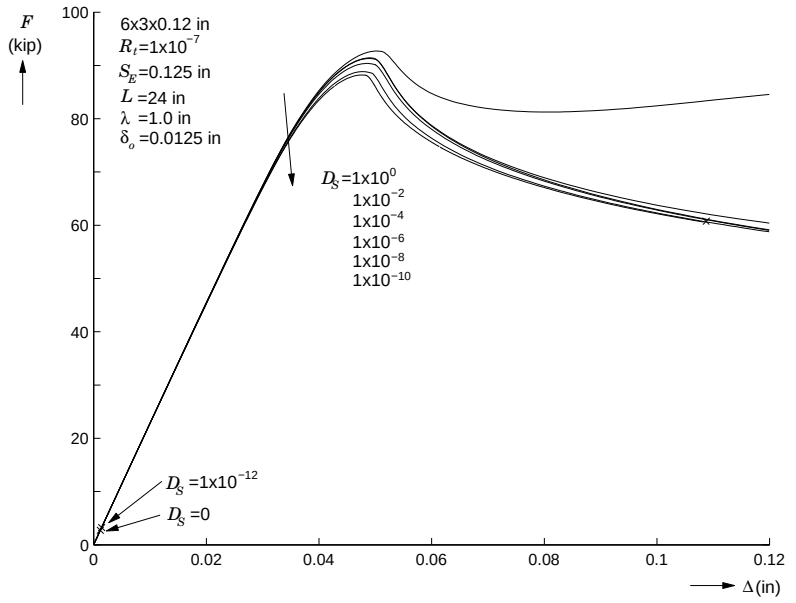

Figure 17. Effect of the value of shell drilling stiffness on the axial load-deflection responses calculated for a 24 in. long, elastic-plastic $6 \times 3 \times 0.12$ in. tubes.

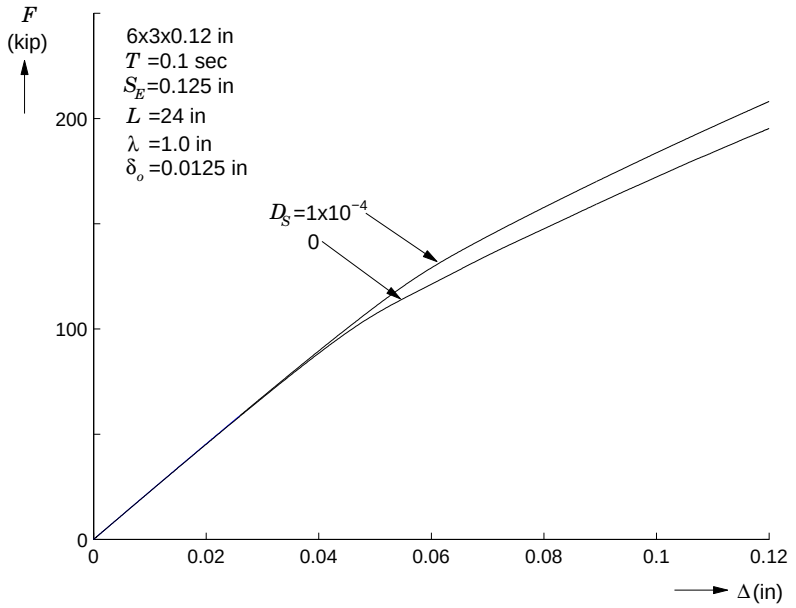

Figure 18. Calculated axial load-deflection response for a 24 in. long, elastic $6 \times 3 \times 0.12$ in. tube calculated using Presto with two values of shell drilling stiffness factor.

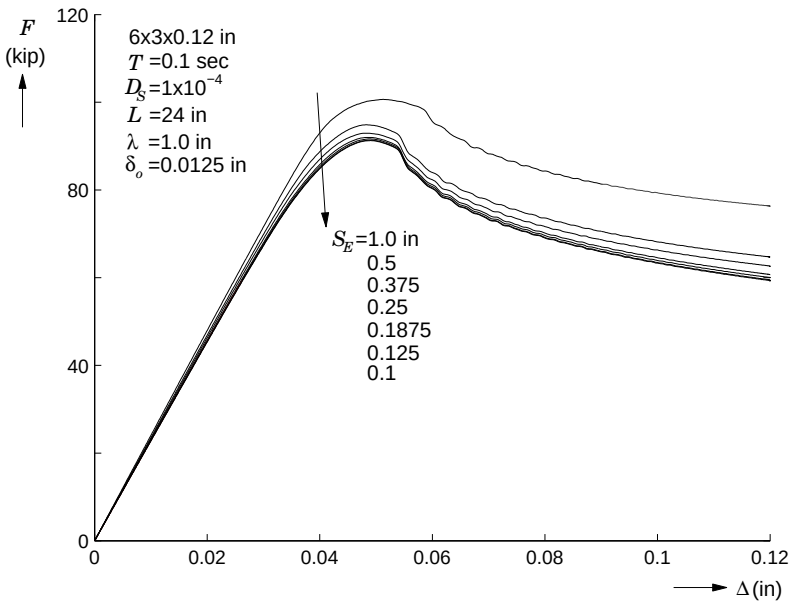

Figure 19. Comparison of axial load-deflection responses calculated for a 24 in. long, elastic $6 \times 3 \times 0.12$ in. tubes with different element sizes using Presto.

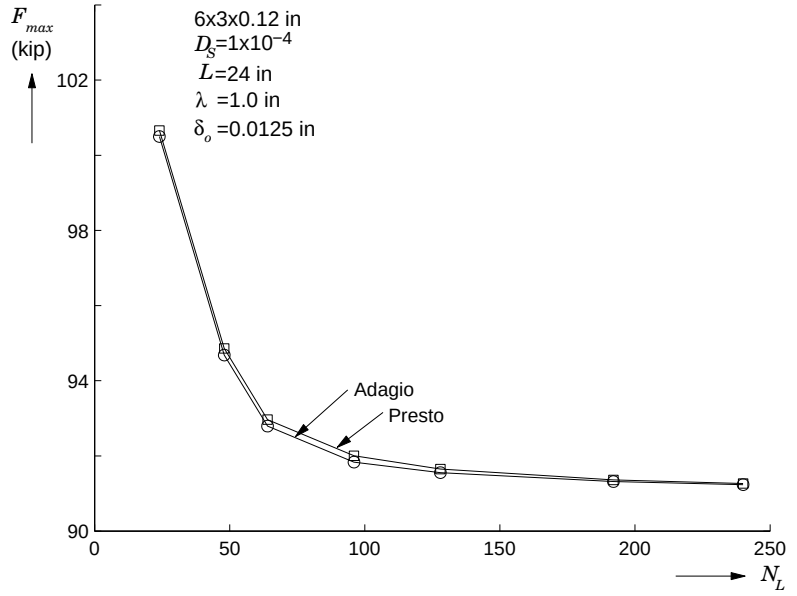

Figure 20. Comparison of the limit loads predicted for 24 in. long, $6 \times 3 \times 0.12$ in. tubes by Adagio and Presto for different element sizes.

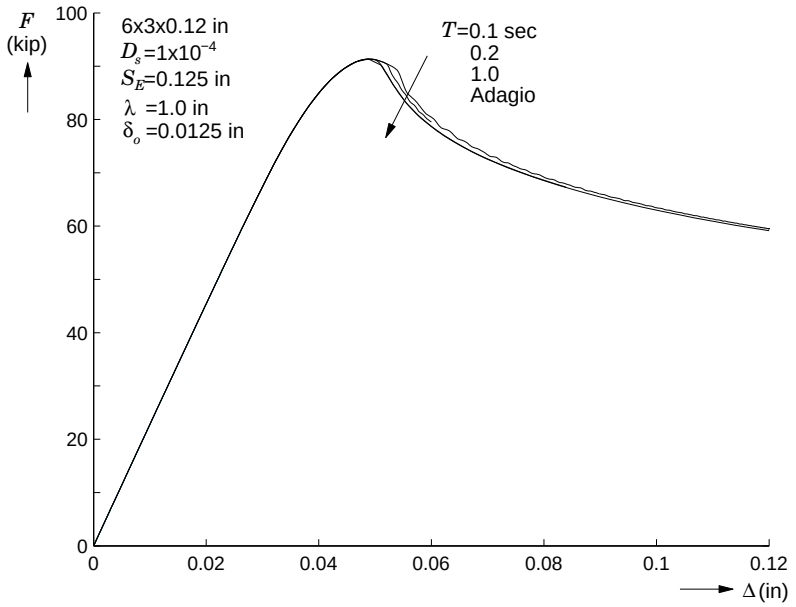

Figure 21. Comparison of axial load-deflection responses calculated for a 24 in. long, elastic $6 \times 3 \times 0.12$ in. tubes using Presto and different time periods. The curve with $T = 1$ s is essentially identical to that given by Adagio.

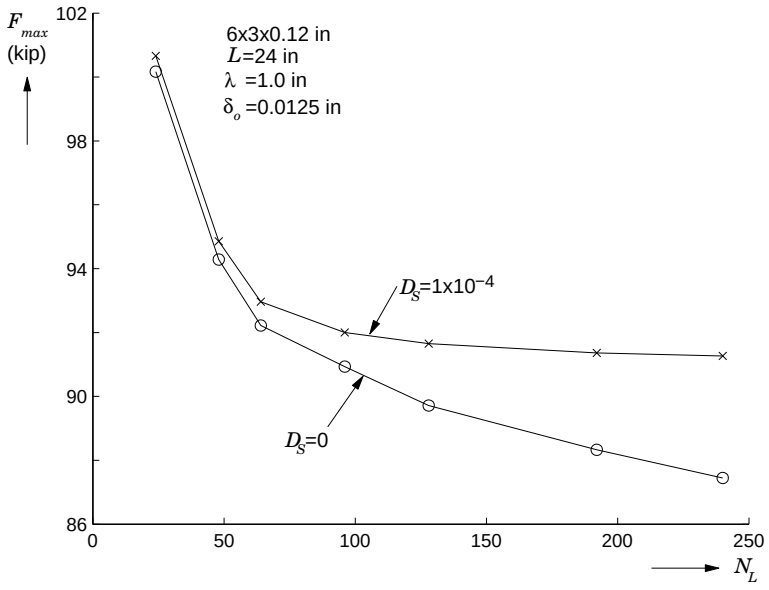

Figure 22. Comparison of the limit loads predicted for 24 in. long, $6 \times 3 \times 0.12$ in. tubes by Presto with the shell drilling stiffness factor set to 1×10^{-4} and zero.

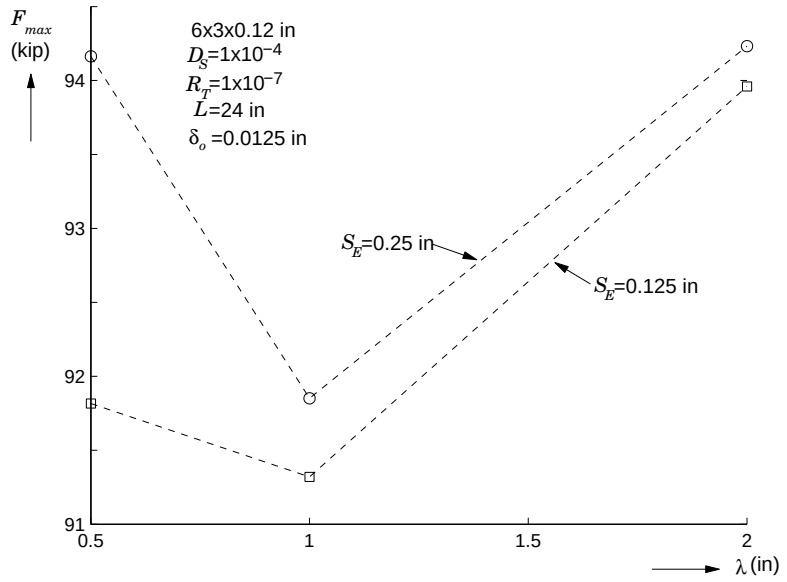

Figure 23. Sensitivity of the collapse load of 24 in. long, $6 \times 3 \times 0.12$ in. tubes to the wavelength of the initial imperfection.

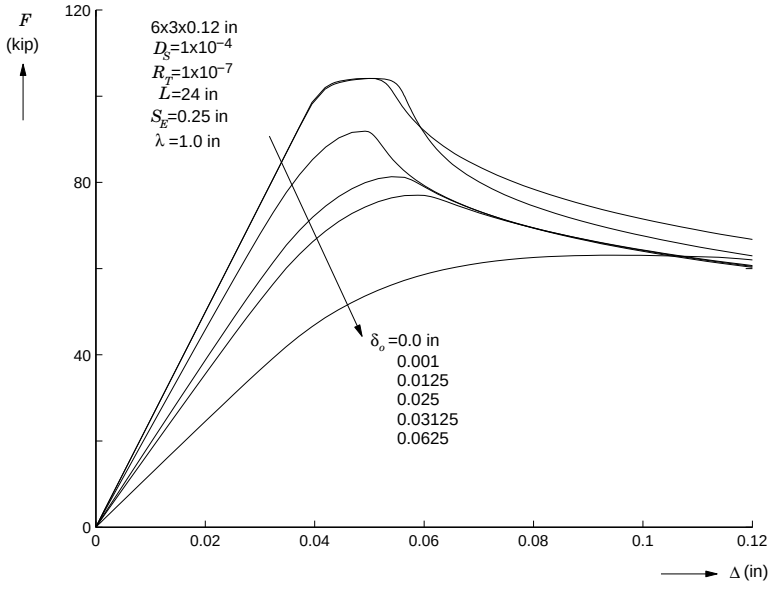

Figure 24. Sensitivity of the axial load-deflection response of 24 in. long, $6 \times 3 \times 0.12$ in. tubes to the amplitude of the initial geometric imperfection.

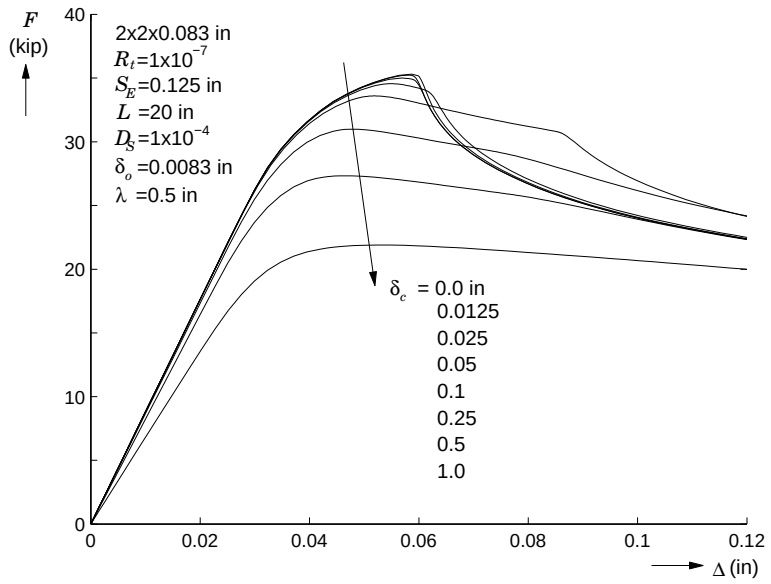

Figure 25. Axial load-deflection responses for 20 in. long, $2 \times 2 \times 0.083$ in. tubes with constant wrinkle imperfection and various column-buckling mode type imperfection amplitudes.

(a)

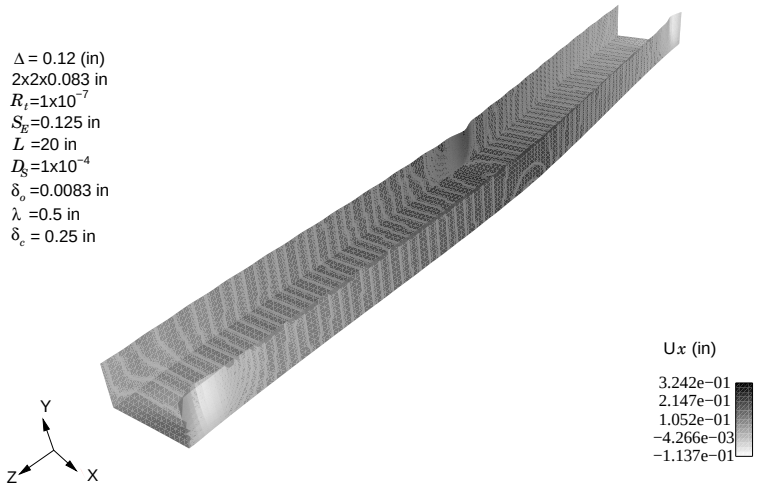

(b)

Figure 26. Shapes of 20 in. long, $2 \times 2 \times 0.083$ in. columns with $\delta_o = 0.0083$ in. but different column-buckling type lateral initial imperfections at $\Delta = 0.12$ in. (a) $\delta_c = 0.0125$ in. and (b) $\delta_c = 0.25$ in.

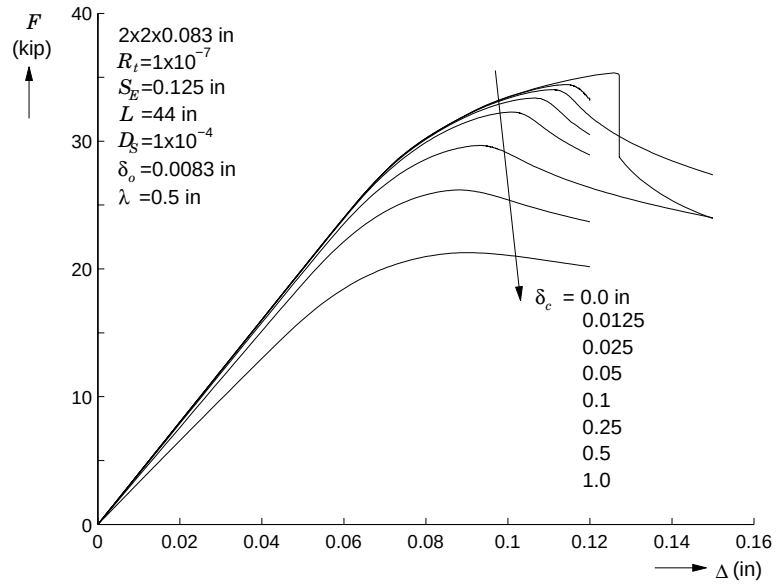

Figure 27. Axial load-deflection responses for 44 in. long, $2 \times 2 \times 0.083$ in. tubes with constant wrinkle imperfection and various column-buckling mode type imperfection amplitudes.

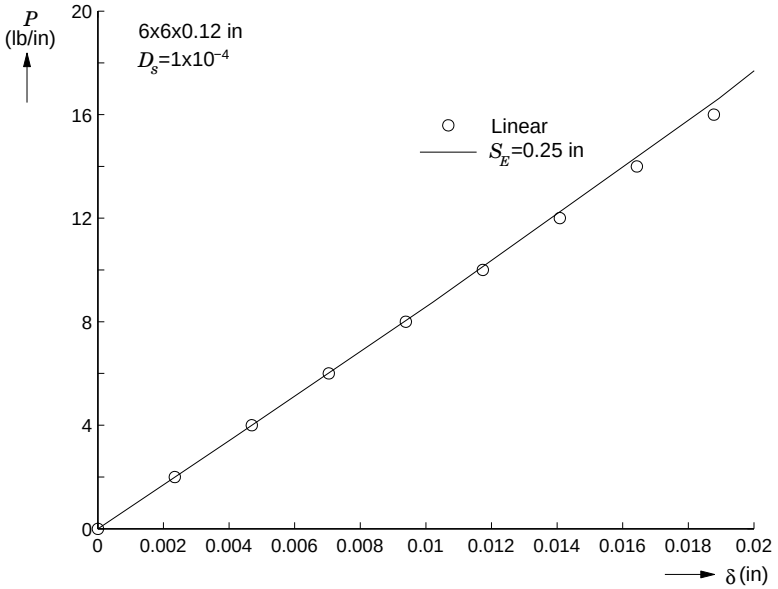

Figure 28. Comparison of the pressure vs. lateral deflection calculated using Adagio against the linear solution (9) for small deflections.

DISTRIBUTION:

1	MS	0372	Edmundo Corona, 1524
1	MS	0372	Jhana Gorman, 1524
1	MS	0380	Jason Hales, 1542
1	MS	0847	Pete Wilson, 1520
1	MS	0372	Nicole Breivik, 1524
1	MS	0372	Eliot Fang, 1524
1	MS	0372	Kenneth Gwinn, 1524
1	MS	0372	David Lo, 1524
1	MS	0372	Kurt Metzinger, 1524
1	MS	0372	Bill Scherzinger, 1524
1	MS	0372	Kristin Dion, 1525
1	MS	0372	Jeff Gruda, 1525
1	MS	0372	Arne Gullerud, 1525
1	MS	0372	Greald Wellman, 1525
1	MS	0372	Frank Dempsey, 1526
1	MS	0346	Dave Reedy, 1526
1	MS	0380	Martin Heinstein, 1542
1	MS	0380	Joseph Jung, 1542
1	MS	0380	Jesse Thomas, 1542
1	MS	0828	Martin Pilch, 1545
1	MS	9042	Mike Chiesa, 8249
1	MS	9042	Mien Yip, 8249
1	MS	0899	Technical Library, 9536 (electronic)

Sandia National Laboratories